Chinese Chemical Letters 34 (2023) 108103

Contents lists available at ScienceDirect

Chinese Chemical Letters

journal homepage: www.elsevier.com/locate/cclet

Extensible and swellable hydrogel-forming microneedles for deep point-of-care sampling and drug deployment

Yuan Liu[a,b], Ting Huang[c], Zhiyong Qian[c,*], Wei Chen[a,b,*]

[a] Department of Pharmacology, School of Basic Medicine, Tongji Medical College, Huazhong University of Science and Technology, Wuhan 430030, China
[b] Hubei Key Laboratory for Drug Target Research and Pharmacodynamic Evaluation, Huazhong University of Science and Technology, Wuhan 430030, China
[c] State Key Laboratory of Biotherapy and Cancer Center, West China Hospital, Sichuan University, Collaborative Innovation Center for Biotherapy, Chengdu 610041, China

ARTICLE INFO

Article history:
Received 29 September 2022
Revised 20 November 2022
Accepted 12 December 2022
Available online 26 December 2022

Keywords:
Dynamic shape alteration
Hydrogel-forming microneedles
Controlled drug released
Biomarker detection
Interaction tunability

ABSTRACT

Microneedles are considered to be an effective, convenient, non-invasive, biosafety and compliant medical technology for vaccinations, biomarker testing, medical aesthetics and other related fields. Nonetheless, further clinical and commercial translation of regular microneedles is hampered by challenges in manufacturability, cost variability, insufficient comfort, contamination and so on. Recent innovations in functional biomaterials and chemical engineering technologies have been applied to develop extensible and swellable hydrogel-forming microneedles, achieving precise and controlled drug delivery and localized sampling from the target tissues. In this review, we systematically summarize the latest development of the extensible and swellable hydrogel-forming microneedles, including deep point-of-care testing, drug deployment, wound healing and mucoadhesion improvement. In addition, further analysis of the challenges and prospects for clinical application of current strategies is well presented. It is believed that the combined efforts of engineering, material, pharmaceutical and clinical research will contribute to the future success of this clinical and commercial translation.

1. Introduction

Microneedles (MNs) are a promising and innovative transdermal drug delivery system with excellent permeability and functional diversity [1]. According to the materials and structures, MNs are mainly divided into 4 categories (solid, coated, hollow and dissolving MNs), which are extensively applied in the fields of tumor therapy, vaccine delivery, biomarker detection, and biosensing [2–4]. However, the solid MN delivery involves a two-step process known as the "poke and patch" method, which dramatically reduces patient compliance [5]. Besides, the direct deposition of the drug to the surface of the coated MNs significantly reduces the mechanical strength and sharpness of the needle, limiting the drug load to a low level [6–8]. In addition, the hollow MNs are prone to undergo blockage by skin tissue and spillage of the drug out of injecting site [4,9-12]. Notably, the main components of those MNs, such as silicon, glass, ceramics, metal, and stainless steel, exhibited relatively low biocompatibility with a high fracture rate, which brings potential risks to the human body and limits their further development [13–16]. Although dissolving MNs with drugs encapsulated in a water-soluble polymer matrix is able to reduce the risk, the potential for partial deposition of the polymer in the skin after dissolution *in vivo* to form granules or erythema is also a non-negligible problem [17,18].

To overcome the limitations of traditional MNs design, extensible and swellable hydrogel-forming microneedles (ES-HFMs) were proposed, which rely on the deformation effect of hydrogels to produce a continuous, non-blocking pathway from the drug reservoir to the microcirculation within the dermis [19–21]. Consisting of cross-linked hydrogel polymers with dynamic deformation properties based on polymer chain relax, ES-HFMs feature a distinct operating mechanism to other conventional MNs (Fig. 1). The hydrophilic nature of the hydrogel polymer allows the ES-HFMs to swell and extend upon insertion into the skin, imparting a deep interaction between the system and local tissues. Alternatively, ES-HFMs offer the possibility of smart drug deployment, by regulating the ratio of polymeric crosslinkers to achieve controlled drug release [22–26]. Importantly, the hydrogel fabrication is flexibly amendable, as the system with various mechanical properties could be adjusted by formulation alteration and dimension restriction [27–31]. Furthermore, the hydrogel systems surmount the biocompatibility problems of silicon or metal MNs while allowing for

* Corresponding authors.
E-mail addresses: anderson-qian@163.com (Z. Qian), weichen86@hust.edu.cn (W. Chen).

https://doi.org/10.1016/j.cclet.2022.108103
1001-8417/

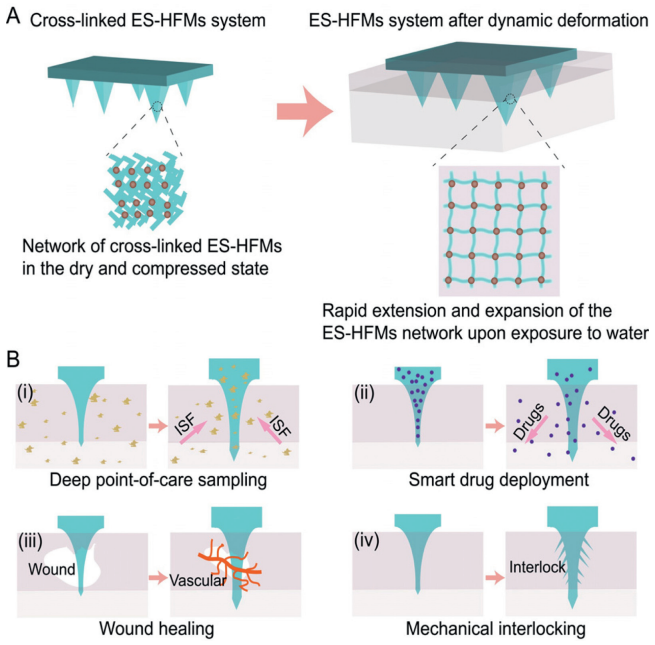

Fig. 1. Schematic representation of the dynamic deformation of ES-HFMs. (A) Rapid extension and swelling of the compressed network of ES-HFMs when exposed to water, demonstrating excellent dynamic shape alteration capabilities. (B) Typical ES-HFMs applications including deep point-of-care sampling, smart drug deployment, wound healing and mechanical interlocking are illustrated.

completed removal from the skin or full dissociation with significant biosafety [32–36]. Evidently, ES-HFMs hold enormous scope for biomedical applications, as in minimally invasive methods of extracting interstitial skin fluid (ISF) for biomarker detection. In this review, we systematically summarized the recent development of ES-HFMs based on advances in the fields of chemistry, medicine and engineering. Initially, the design and fabrication strategy of ES-HFMs was described in detail, especially in terms of bionics and engineering inspiration. Subsequently, the application of the ES-HFMs was depicted with emphasis on the potential in deep point-of-care testing and drug deployment. Furthermore, the challenges and prospects, including biosecurity and clinical translational potential, were discussed in depth. It is believed that the ES-HFMs will be a promising candidate in industrial and clinical fields, indicating great potential in healthcare providers and patients in the near future.

2. ES-HFMs fabrication

2.1. Materials for ES-HFMs

During the ES-HFMs fabrication, diverse polymers serve as crucial components as a result of their gelling capability, which effectively improves the mechanical strength of the system and facilitates controlled drug release, as well as dynamic shape alteration [29,37-39]. The materials include natural polymers (*e.g.,* hyaluronic acid, gelatin, agar, silk protein) and synthetic polymers (*e.g.,* polyvinyl alcohol, sodium polyacrylate, poly(methacrylic acid), acrylic resin, polyvinyl pyrrolidone), can generate a broad spectrum of hydrogels by a physical connection, electrostatic interaction or chemical cross-linking between molecules [40]. For example, Guozhong Yang *et al.* utilized acrylic resin to develop ES-HFMs with satisfactory mechanical properties and drug loading capacity, which greatly improved the release of water-insoluble drug, granisetron base [41]. Further studies revealed that the system obtained a 7-day controlled release of granisetron base when involving porogenic agents (1.5% dicalcium phosphate and 1.5% polyvinyl pyrrolidone). Meanwhile, the maximum drug amount entering the skin was 86.158% ± 7.82% of the initial granisetron base (2.1 mg), suggesting that systems incorporating appropriate polymeric materials offer a minimally invasive route but deep penetration and amount of drug deployment. Interestingly, it was found that certain polymers are able to smartly respond to the microenvironmental stimuli including pH, light or temperature, exhibiting significant dimension changes through swelling, expansion, sol-gel transition and network re-structuring. For instance, John G. Hardy *et al.* prepared stimulus-responsive HFMs using 2-hydroxyethyl methacrylate and ethylene glycol dimethacrylate, which are capable of delivering clinically used model drugs (ibuprofen) under light stimulation through spontaneous swelling (Fig. 2) [42]. Notably, this type of material was found to be more suitable for long-acting drug delivery due to the controllable and adjustable swelling processes.

2.2. Engineering structure of ES-HFMs

Due to the heterogeneity of the skin and unavoidable movement during puncture, ES-HFMs are subject to a variety of mechanical interactions, leading to fracture, bending, and other deformations, which affect the puncture performance [26,35,43,44]. Therefore, besides the matrix material, the engineering structure of the MNs such as length, shape, density, and spacing distance between each needle play a significant role in the penetration and removal processes [45–47]. The length of the MNs needs to be optimized to guarantee that the needles penetrate the skin whilst avoiding touching the underlying nerve endings, hence most MNs are approximately 25 μm to 2500 μm in length, 50 μm to 250 μm in width, and 1 μm to 25 μm in tip diameter [48]. Over-dense MNs would result in a "bed of nails" effect, which makes it difficult to effectively break through the stratum corneum barrier. At the same time, it decreases the MNs spacing, which remarkably reduces the penetration rate especially when the spacing is below 150 μm. According to a recent study, a density of fewer than 2000 needles/cm^2 would be more favorable in terms of effective skin penetration [49,50]. For example, Zequan Zhou *et al.* constructed a Ca^{2+} cross-linked alginate ES-HFMs (round, 500 μm height, 500 μm spacing, 145 tips), which significantly improved the drug transdermal penetration, especially for acidic drugs [51]. Noticeably, differences in matrix materials, geometry parameters, and applicable targets may lead to variations in results, a further systematic exploration is still necessary to study the relationship between engineering structure and ES-HFMs performance to provide sufficient controllability, effectiveness and safety.

Recently, bionics has gained substantial interest in the ES-HFMs fabrication, which inspired scientists and engineers to optimize the structure and shape layout of MNs by simulating the unique physiological and functional properties of living organisms [52,53]. Based on the biological surface wetting, adhesion, and friction mechanisms, the combination of the mechanics, materials science, mechanical design and manufacturing science, achieves great success in surface wetting, adhesion adjustment, resistance enhancement, and wear tolerance [54]. The stinging-sucking mouthparts of mosquitoes, gadflies, bees, cicadas and other insects have been extensively studied and serve as bionic prototypes of MNs due to their promising epidermis penetration and smart interactions [55–57]. Interestingly, in nature, some internal parasites have evolved to adhere to the host's intestinal wall by utilizing special components (*e.g.,* hooks or suckers). *Pomphorhynchus laevis*, known as the spiny-headed worm, uses an expandable proboscis to hold firmly in the parasitic position after penetrating the intestinal wall [58]. Utilizing this principle, Eun Young Jeon *et al.* designed a biomimetic swellable hydrogel bilayer MN that achieves excellent tissue adhesion and closure under wet and/or dynamic conditions

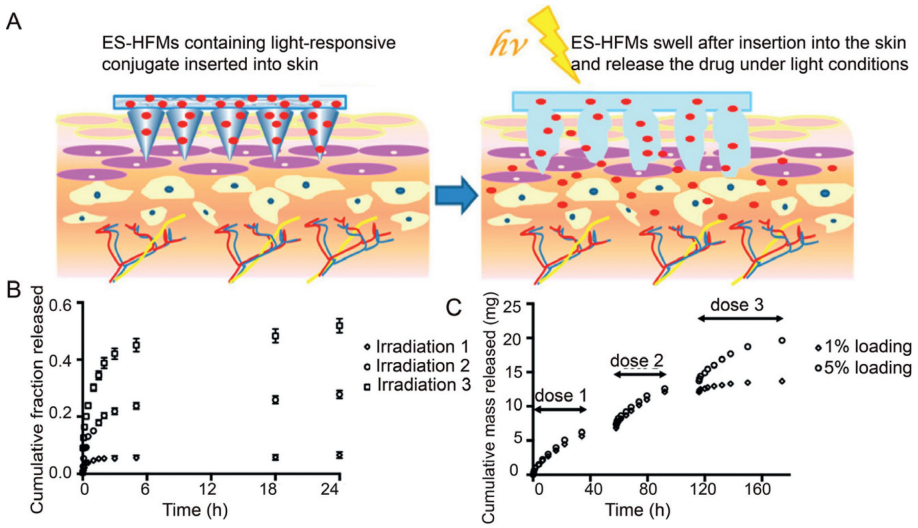

Fig. 2. Materials for ES-HFMs. (A) Schematic representation of drug release from ES-HFMs made from light-responsive materials. (B) Cumulative fractional release profiles of ibuprofen from 3 × 3 ES-HFMs loaded with photoresponsive couplers over 3 irradiation cycles (irradiation 1/2/3) after 1 h of continuous irradiation at 365 nm. (C) Ibuprofen release from 3 × 3 ES-HFMs with release triggered by 3 cycles (dose 1/2/3) of exposure to light for 1 h. The 1% and 5% loading are ES-HFMs containing 1% and 5% light-responsive couplers. Copied with permission [42]. Copyright 2016, the American Chemical Society Publications.

through surface adhesion and selective swellability of the hydrogel (Fig. 3) [32].

2.3. Bioactive nanocomponents of ES-HFMs

MN-mediated drug release generally relies on passive diffusion, where external stimuli (*e.g.,* ultrasound, light, temperature) are often employed to improve drug delivery, avoiding the low penetration and uneven distribution of therapeutic agents [59,60]. For example, Lu Fan *et al.* proposed a strategy for versatile and controlled drug delivery by integrating photoresponsive drug delivery microspheres into pyramidal MNs [61]. Benefiting from the sufficient water content of the swellable hydrogel, the MN was able to load various bioactive substances with well-maintained biological activity, which could be delivered to a deeper location at the target site. Nevertheless, the demand of bulky external equipment limits its application as a result of the troublesome operation, specialist handling and high cost. Further efforts are thus necessary to incorporate the merits of autonomous and active drug delivery into a simple MN delivery platform, while decreasing the time and cost required to achieve significant therapeutic efficiency. Recently, nano-scaled components were encapsulated into the ES-HFMs to endow them with autonomous bioactive properties, facilitating the MN extension and drug diffusion. As an illustration, Miguel Angel Lopez-Ramirez *et al.* described a swellable hydrogel-based bioactive MN delivery platform loaded with a therapeutic payload and active motor magnesium (Mg) microparticles, which was capable of generating autonomous intense convective fluid flow to improve drug deployment (Figs. 4A-D) [62]. As the polymer matrix dissolves within the skin, the embedded magnesium particles were exposed and react instantly with the surrounding ISF to rapidly produce hydrogen bubbles (Fig. 4E). These microbubbles induce a powerful and autonomous swelling pumping effect, and thus result in dynamically and extremely efficient transport and penetration of the embedded therapeutic payload. *In vitro* evaluation using fluorescence dye as a model drug revealed that the encapsulated Mg particles greatly enhanced the effective loading and delivery of the model dye within 5 min compared to the delayed delivery of passive MNs (without Mg particles). This phenomenon was significantly more pronounced at 10 min, where the passive MN resulted in a mean depth of 111 ± 79 μm *versus* 526 ± 71 μm with the active MN (Fig. 4F). Distinctively, the active delivery strategy of ES-HFMs offers considerable promise for rapid and deep drug deployment with a sophisticated design and bioactive nanocomponent integration.

3. Biomedical application of the ES-HFMs

Nowadays, the HFMs have been extensively studied and exhibited great potential in deep point-of-care sampling, smart drug deployment, wound healing, mechanical interlocking, *etc.* (Table 1). Currently, the most widespread approach for ES-HFMs fabrication should be the micro-modeling, in which the polymer solution was filled into the prepared microneedle array mold by external forces such as heating, centrifugation, evacuation, and light-mediated crosslinking to form the microneedle array (Fig. 5). As an illustration, Na Xu *et al.* prepared swellable polyvinyl alcohol/polyvinylpyrrolidone hydrogel microneedle patches by casting the polymer solution into the polydimethylsiloxane (PDMS) molds followed by careful removal, which perfectly maintained the morphology and were able to penetrate the skin in the dry state to extract ISF [26]. Furthermore, in order to minimize tissue damage while achieving significant adhesion to soft tissues, Yun Yang *et al.* applied a similar method to create a stimulus-responsive bilayer microneedle *via* double casings of block polyacrylic acid (PS-*b*-PAA) block copolymer and polystyrene (PS) [58]. Briefly, when PS-*b*-PAA solution was added into a PDMS mold, capillary forces would induce a thick film near the conical cavity's tip, while a thin film was generated elsewhere on the mold surface. Subsequently, the PS homopolymer was then melted on top of the intact PS-*b*-PAA layer, and the microneedle patch was peeled from the PDMS after cooling to the room temperature.

3.1. Deep point-of-care sampling

Interstitial skin fluid (ISF) containing a wealth of biological information is an ideal sample resource for point-of-care testing; however, collecting sufficient markers in ISF in a minimally invasive or non-invasive manner remains a great challenge [63,64]. In recent years, solid and hollow MNs have attracted growing attention in ISF sampling by facilitating fluid transport due to the capillary action [65]. Nevertheless, these systems are mainly made of silicon, glass and metal, which suffer from fragility, environmen-

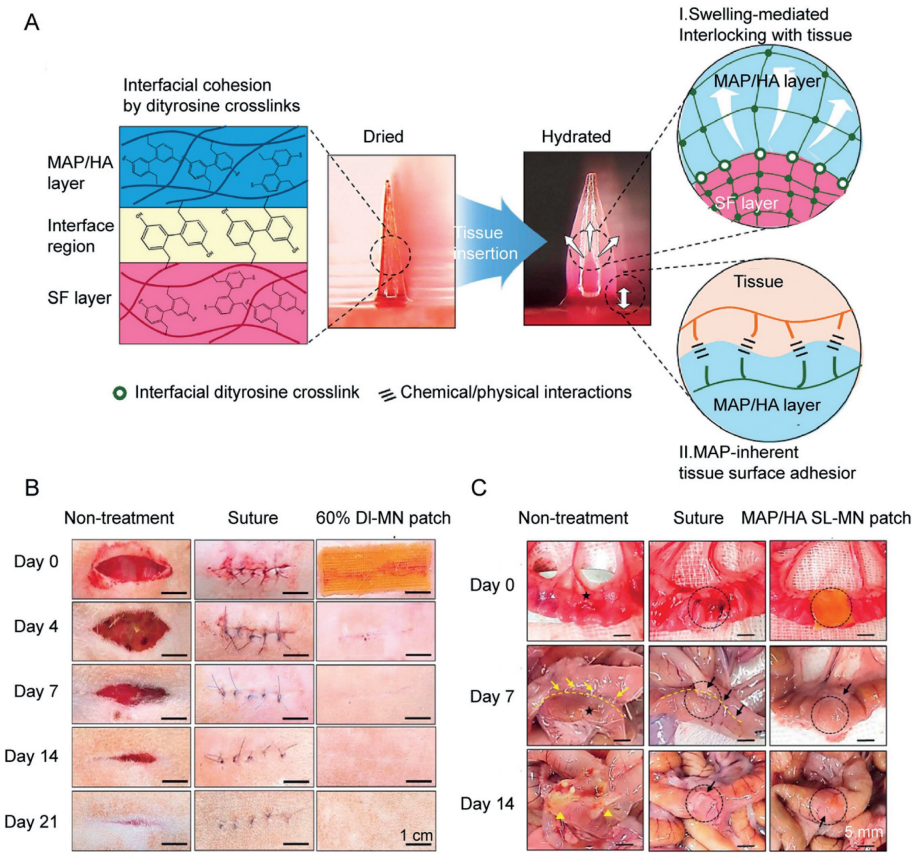

Fig. 3. Engineering structure of ES-HFMs. (A) Schematic diagram of the working mechanism of ES-HFMs, a patch consisting of a swellable and adhesive mussel adhesive proteins (MAP)-based shell and a non-swellable silk fibroin (SF)-based core. (B) Macroscopic images of rat skin wound healing after non-treatment, suture treatment and 60% double-layered MN (DL-MN) treatment. (C) Macroscopic images of a 5 mm diameter defect in the rat ileum after untreated, suture-treated and mussel adhesive protein/hyaluronic acid single-layered MN (MAP/HA SL-MN) treatment. Defect (black star), treated site (black dashed circle), the border between attached bowel (yellow dashed line), adhesion site indicating intestinal canal (yellow arrow), fatty attachment (black arrow) and leakage (yellow triangle). Copied with permission [32]. Copyright 2019, the Elsevier.

Table 1
Typical ES-HFMs and their applications.

Materials	Arrays				Application	Ref.
	Height (μm)	Diameter (μm)	Tip distance (μm)	Array		
Methacrylate hyaluronic acid	800	250	450	10 × 10	Extraction of ISF	[21]
Polyvinyl alcohol/polyvinylpyrrolidone	600/800/1000	300/440/500	500/600/650/1000	10 × 10	Monitoring of glucose	[26]
Gelatin methacrylate	300-700	-	150-1000	15 × 15	Monitoring kidney disease	[31]
Maltose, methacrylated hyaluronic acid	550	200	500	15 × 15	Monitoring of glucose	[35]
Silk fibroin	900	280	-	-	Transdermal delivery of glucose	[36]
Polyethylene glycol	600	300	50	19 × 19	Antipyretic and analgesic	[69]
Silk fibroin, phenylboronic acid/acrylamide	700	-	-	10 × 10	Delivery of insulin	[73]
Alginate	500	-	500	-	Delivery of acidic drugs	[51]
Polystyrene	700	280	-	10 × 10	Skin graft fixation	[58]
Mussel adhesive protein	750	250	750	10 × 10	Regenerative internal/external surgical closure	[32]

tal pollution, complicated preparation process, high cost and short skin micropore opening time. Moreover, in order to speed up the extraction process and obtain sufficient ISF, multiple steps and additional devices to provide negative pressure are often required, severely increasing the complexity and risk of infection for the user. Therefore, it is particularly important to continuedly develop user-friendly and commercially MNs for deep point-of-care testing.

The specific phase change properties of hydrogels (stiff in drying, soft after absorbing water) result in accessible skin penetration, extensible and swellable capabilities, perfectly suitable for non-pump ISF extraction [66]. Rongyan He *et al.* developed a point-of-care testing platform based on polyvinyl alcohol/chitosan hydrogel MNs, which allowed for quick extraction of rabbit skin ISF, the release of target biomarkers and analysis of their concentrations by colorimetric assay (darker color indicated higher glucose concentration) in a short time without any bulky instrumentation (Figs. 6A-C) [67]. It was observed that the ISF extracted from rabbits by this system increased with the extraction time and reached 1.25 ± 0.37 mg after 10 min (Fig. 6D). Meanwhile, the accuracy of ES-HFMs-based test was compared to hematological testing in terms of blood glucose level (BGL) which was performed using a commercial glucose meter, indicating excellent consistency between the measurements with the similar BGL range (4-14 mmol/L) (Fig. 6E). This phenomenon has also been verified in other biomarker detection (lactic acid, urea, *etc.*), suggesting that the ES-HFMs platform was capable of enhancing the point-of-care sampling with satisfactory accuracy, and without undesirable drawbacks of blood-related sampling, including vascular

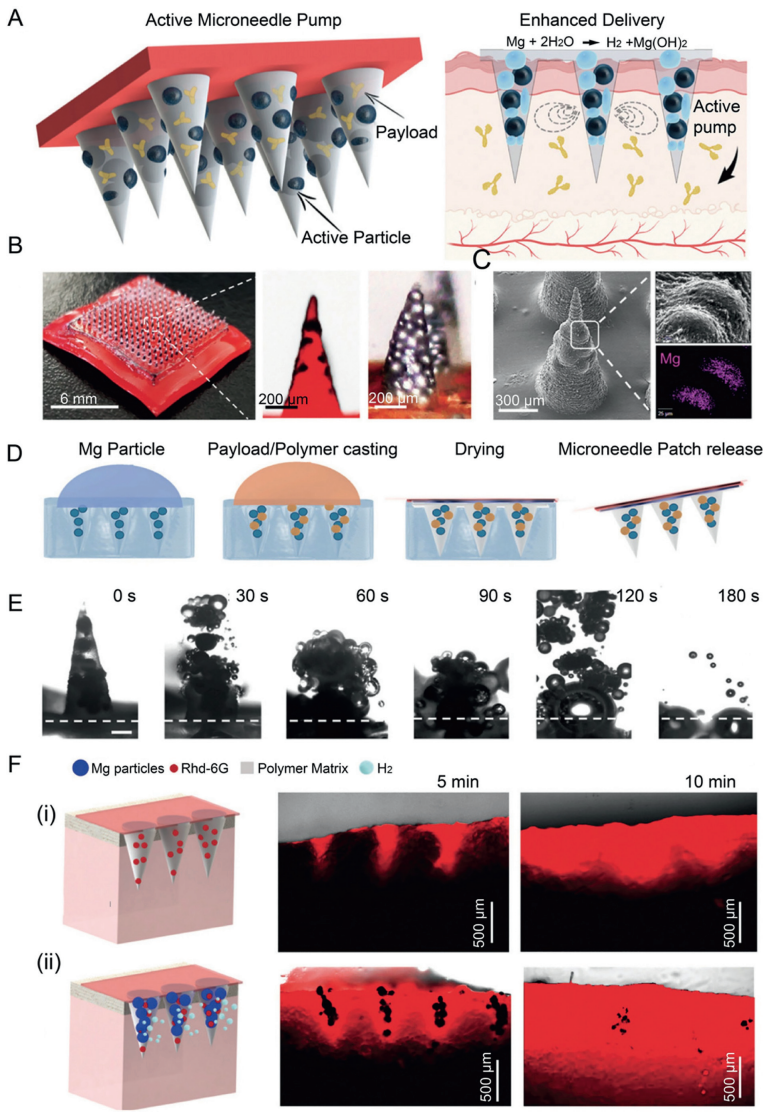

Fig. 4. Bioactive nanocomponents of ES-HFMs. (A) The active MN patch component, as well as the built-in Mg particles that act as a pump when in contact with body fluids, are activated, thus enhancing drug release. (B) Digital photograph showing an optical/fluorescent microscope image of a 15×15 MN array and an active MN tip. (C) SEM image of a single active MN tip and EDX analysis of Mg. (D) Manufacturing steps for MNs: poly(dimethylsiloxane) microforming on the primary MN, poly(dimethylsiloxane) negative MN demolding, Mg particle loading, polymer and payload inclusion, polymer drying, adhesive application and peeling. (E) Microscope time frame image is taken from a single reactive MN point, clearly showing the dissolution of the polymer in PBS pH 6.0 and the activation of the particles (at 30-second intervals). (F) Schematic diagram illustrating the experimental set-up of passive (i) and active (ii) MNs penetrating pig skin, and cross-sectional images of fluorescence microscopy at different times. Copied with permission [62]. Copyright 2020, the Wiley.

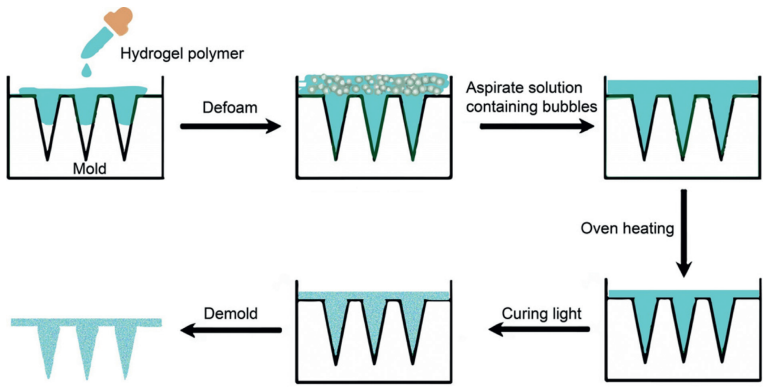

Fig. 5. The typical manufacturing process of ES-HFMS *via* micro-modeling.

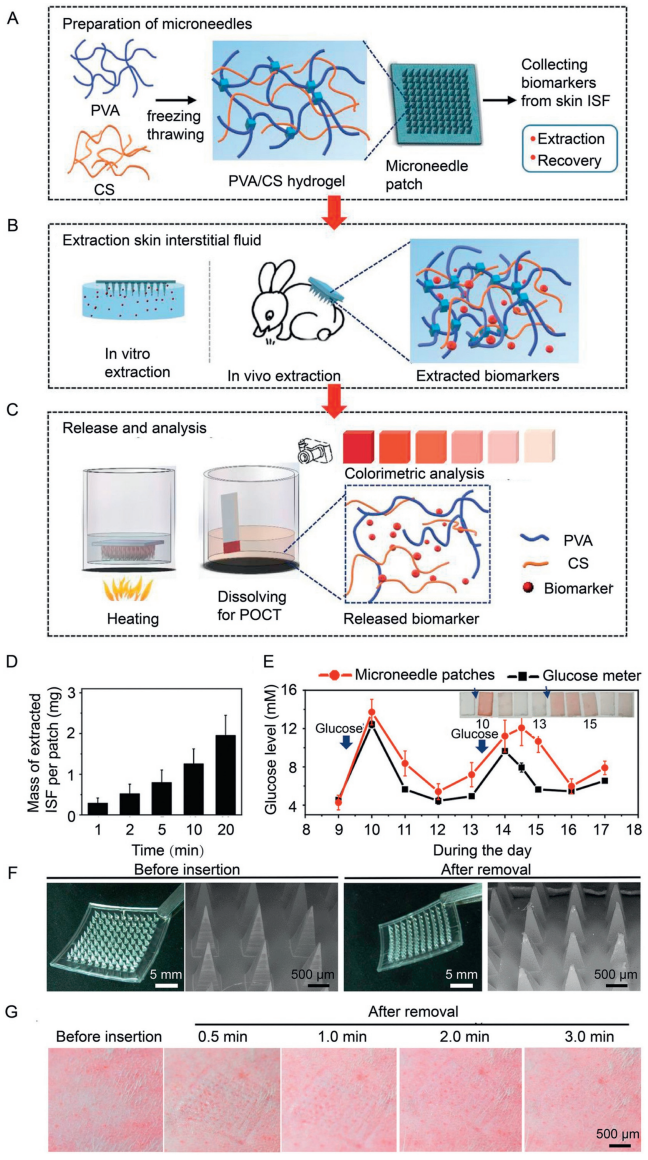

Fig. 6. Application of ES-HFMs for deep point-of-care sampling. (A) Preparation of PVA/CS hydrogel ES-HFMs. (B) Target biomarkers were extracted from simulated skin *in vitro* and rabbit dorsal skin *in vivo*. (C) Recovery of target biomarkers from ES-HFMs by heating and detection using a colorimetric assay (darker color indicated higher glucose concentration). (D) The mass of ISF extracted from rabbits by the patch increased with extraction time and reached 1.25 ± 0.37 mg after 10 min. (E) Glucose levels obtained by ES-HFMs and a commercial glucose meter were excellent consistent in terms of quality and quantity. (F) Images before and after insertion of ES-HFMs into the skin of rabbits showing no breakage despite a slightly blunted needle tip. (G) Microchannels on the skin surface of the rabbit's back disappeared rapidly within 3 min after removal of ES-HFMs. Copied with permission [67]. Copyright 2020, the Wiley.

damage, bacterial infections, painful sensations, needle fear and self-administration challenges [40]. Afterward, insertion of the ES-HFMs into the skin of the rabbits revealed no breakage despite a slightly blunted tip, and the micropores disappeared rapidly within 3 min with minimal mechanical damage to the skin (Figs. 6F and G). Not negligibly, certain ES-HFMs still demand a multi-step sequence with high time consumption to gather sufficient volume (1 mL) for valid analysis. In order to simplify the process, Mengjia Zheng *et al.* introduced a swellable hydrogel (methacrylated hyaluronic acid) MN patch powered by an osmolyte (maltose), where the osmolyte dissolved in the matrix and provided osmotic pressure, increasing the diffusion of ISF from the skin to the hydrogel matrix [36]. The system with 100 MNs extracted 7.90 μL of ISF from *in vitro* pig skin and 3.82 μL of ISF from *in vivo* mouse skin within 3 min, whereas the control (hydrogel MNs free of penetrant) required more than 10 min to reach comparable outcomes. Given the latest trends in effortless personal self-medical monitoring, it would be more convenient to involve the biomarker enrichment, collection, release and analysis in one system. Developing automated ES-HFM-based platforms for sample concentration, microfluidics, and quick indication, or combining with other smart devices would be an encouraging strategy in the future point-of-care sampling.

3.2. Smart drug deployment

The extensive property of the ES-HFMs provide enlarged space for drug deployment, which has been successfully employed to improve transdermal delivery of small molecule drugs such as granisetron base, sodium ibuprofen and lidocaine hydrochloride. Ryan F. Donnelly *et al.* developed "super-swelling" HFM containing 20% w/w Gantrez S-97, 7.5% w/w PEG 10,000, and 3% w/w Na_2CO_3, for the delivery of ibuprofen sodium assisted by the lyophilized wafer technology (Figs. 7A-D) [68]. These MN-based freeze-dried wafer compositions solidly and effectively penetrated the skin and swelled remarkably toward deep locations. During *in vivo* test, the system delivered approximately 44 mg of ibuprofen sodium within 24 h, equivalent to 37% of the load in the lyophilized storage solution. Besides, macromolecules were also deployed by this system, where 1.24 mg of ovalbumin was successfully delivered within one day, demonstrating a efficiency of about 49% (Figs. 7E-H). Furthermore, ES-HFMs with sustained drug release had also been invented, where swellable aqueous silk fibroin was fabricated in system with tremendous fidelity and mechanical robustness, allowing easy puncture into pig skin (depth of about 200 μm, and conversion to 50-700 nmol/L semisolid hydrogels with an internal porous network), which exhibited the sustained glucose release due to its gradual degradation [31]. Moreover, Siyuan Chen *et al.* reported a smart MN composed of silk protein and a semi-interpenetrating network hydrogel prepared from phenylboronic acid/acrylamide for glucose-responsive insulin delivery [69]. This smart MN autonomously releases insulin by modulating the skin layer formed on the surface, which corresponds favorably to the glucose variation pattern and promises to deliver on-demand insulin in a long-lasting, painless and convenient manner. It should be noted that nanoparticles (liposomes, microspheres, *etc.*) were frequently employed for subcutaneous drug delivery, but they were mainly compromised by the injection-associated pain, unremovable operation, uncontrollable degradation and limited penetration depth, which were fortunately impro ved by the ES-HFMs systems by offering smart insertion, swell and extension-based features [48,70-72].

3.3. Wound healing

To repair severe tissue damage and skin scars, patches that significantly inhibit bacterial infection and accelerate wound healing are considered to be the most effective candidates [73–78]. Typically, the traditional formulation mainly included various active drugs (*e.g.*, bactericidal, hemostatic, anti-inflammatory, and angiogenic factors) with adjuvants such as diverse nanoparticles [79–82]. Nonetheless, the complex biological and chemical fabrication procedures involved in conventional patches reduce biocompatibility and biosafety, thus further limiting their application in deep tissue injuries. Crucially, the single structure does not confer extensible and swellable dynamic shape alteration properties to the typical patches, and thus fails to provide real-time traction and fixation effects for tissue repair. As a result, it is expected to develop multifunctional patches for wound healing in combination

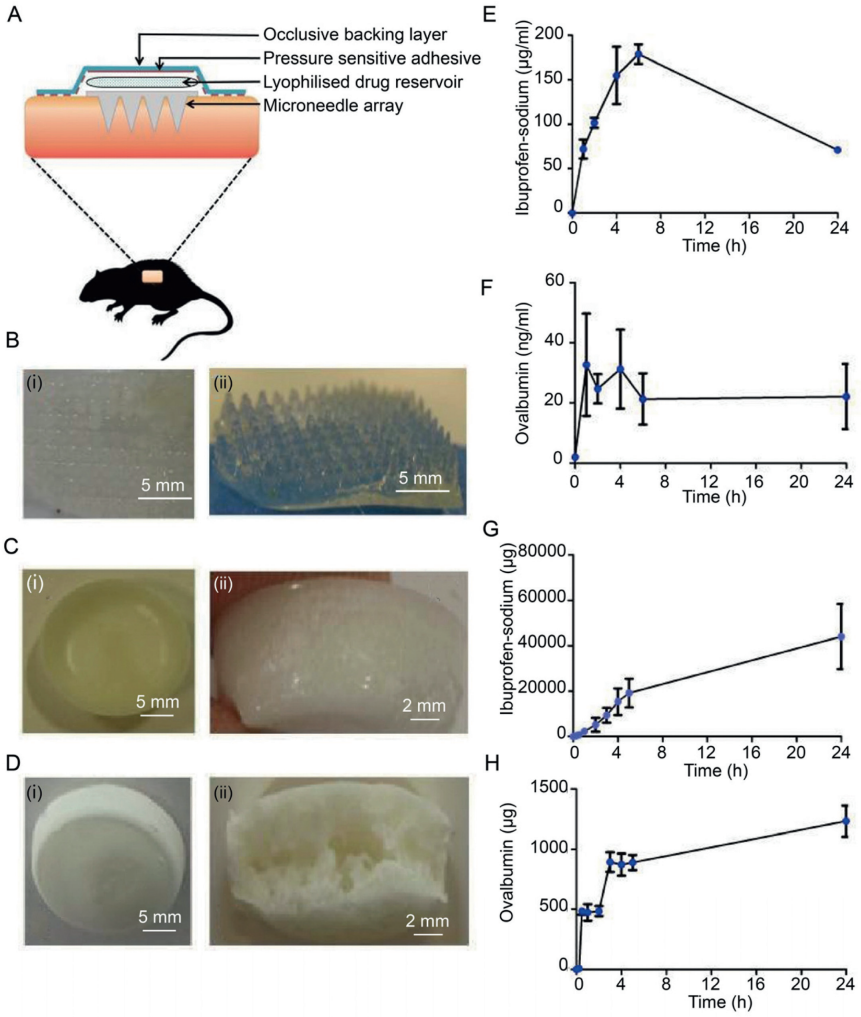

Fig. 7. Application of ES-HFMs for smart drug deployment. (A) Schematic diagram of the application and retention strategy for rat experiments designed to assess the *in vivo* performance of ES-HFMs. (B) After 24 h of insertion, despite extensive swelling, ES-HFMs can still be removed intact from rat skin. (C) Digital image of a lyophilized wafer loaded with sodium ibuprofen. (D) Digital image of lyophilized wafer loaded with OVA. The plasma concentration of ibuprofen sodium (E) and OVA (F) in rats after transdermal administration using ES-HFMs. (G) Cumulative permeation profile of ibuprofen sodium in porcine skin by *in vivo* ES-HFMs combined with a lyophilized drug reservoir. (H) Cumulative permeation profile of OVA in porcine skin by *in vivo* ES-HFMs combined with a lyophilized drug reservoir. Copied with permission [68]. Copyright 2014, the Plos One.

with the tunability of hydrogel interactions and the superior microstructure of MNs [83–88]. Junjie Chi *et al.* invented a biomass chitosan-ES-HFMs by utilizing poly(*N*-isopropylacrylamide) hydrogel as an intelligent temperature responsive system, which was able to encapsulate vascular endothelial growth factor (VEGF) in the micropores [89]. Precisely controlled release of VEGF was achieved through exposure to different temperatures that cause the poly(*N*-isopropylacrylamide) hydrogel to extend/contract, thus accelerating inflammation inhibition, collagen deposition, angiogenesis and granulation tissue formation. Furthermore, Soomee Lim *et al.* proposed a double-layered adhesive MN bandage (DL-AMNB) as a therapeutic cardiac patch, which consisted of a biofunctional mussel adhesive protein-based root and a regenerating filamentous protein-based tip (Fig. 8) [90]. The system evidently displayed better cardiac muscle preservation and wound healing compared to the conventional cardiac patches in a rat myocardial infarction model, possibly owing to highly efficient delivery and long-term retention of the therapeutic peptide (*i.e.*, vascular endothelial growth factor, fibroblast growth factor-2 and extracellular matrix protein), as well as the safe adhesion between the patch and the host myocardium *via* the intense underwater adhesion similar to mussel adhesive protein.

3.4. Mechanical interlocking

Achieving mechanical interlocking effects on soft tissues while minimizing tissue damage is a considerably clinical challenge. Chemical adhesive-based approach requires specific reactive chemistry and may induce a severe inflammatory response [91–95]. Sutures need sophisticated operation by the professional staff, and are not suitable in dura mater, urethral defects, lung tissue and so on [96–100]. Staples are also fraught with limitations including intense local tissue pressure and high infection risk, as well as nerve and vascular damage [101–105]. Unlike ordinary mechanical interlocking means, ES-HFMs have displayed shorter procedure times, decreased scarring rate, dispersed force over a broader surface area, as well as dynamically scalable tissue handling.

Inspired by the swollen proboscis of endoparasites for stable immobilization on host tissue after insertion, Seung Yun Yang *et al.* have developed a biphasic MN that exhibited precise interlocks with the tissue through an expandable MN tip, further developing grip strength by about 3.5 times contrasted with staples in the skin for uniting obsession with an evacuation force about 4.5 N/cm^2 from gastrointestinal mucosal tissue (Fig. 9) [58]. This design minimizes the force required to penetrate the tissue, ensuring

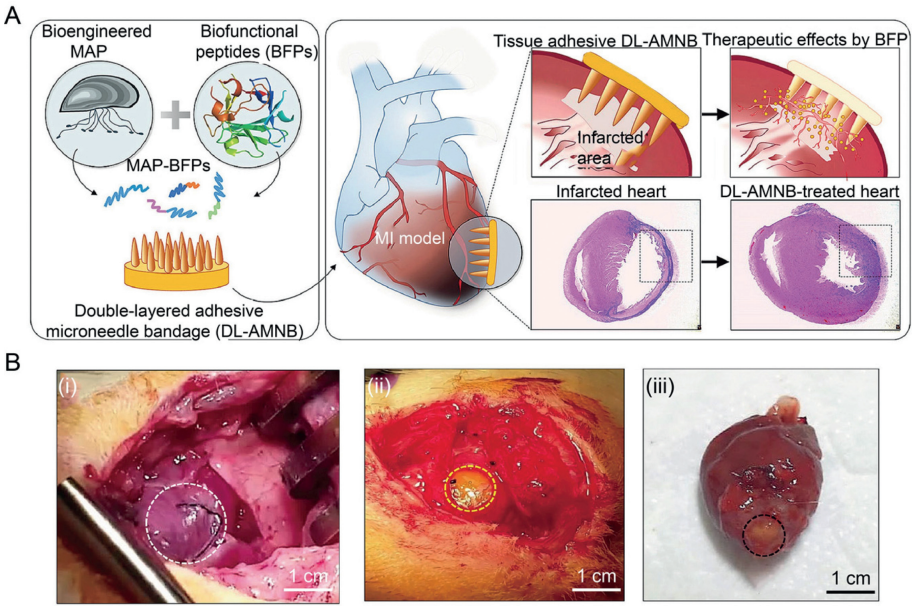

Fig. 8. Application of ES-HFMs for wound healing. (A) Schematic representation of DL-AMNB, including biofunctional peptides fusion mussel adhesive protein for myocardial infarction treatment. (B) *In vivo* DL-AMNB treatment effect in a rat myocardial infarction model. Photographs of DL-AMNB treatment of the infarct zone before (i) and after (ii). The yellow dashed circles represent the infarcted area. (iii) Macroscopic images of the remaining DL-AMNB adhering to heart tissue 2 weeks after treatment. Copied with permission [90]. Copyright 2021, the Elsevier.

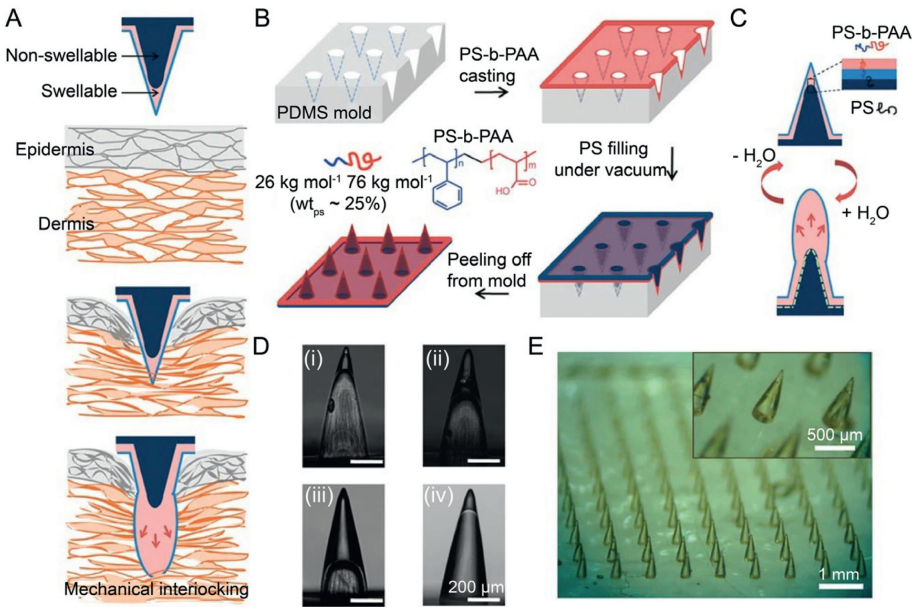

Fig. 9. Application of ES-HFMs for mechanical interlocking. (A) The mechanical interlocking of ES-HFMs after tissue penetration. (B) ES-HFMs were prepared using PDMS molds and show the chemical structure of polystyrene-block-poly-acrylic acid (PS-*b*-PAA), where the weight fraction of polystyrene used for the expandable tip is 25%. (C) Schematic diagram showing the internal structure and reversible water reactivity of a bilayer MN. (D) Side views of hollow MNs (without polystyrene core) with different PS-*b*-PAA filling ratios, including (i) 20%, (ii) 40% and (iii) 70%. (iv) Bilayer MN with expandable tip after filling with polystyrene core. (E) Photograph of ES-HFMs at a density of 10×10 cm^{-2}, showing high pattern fidelity. Copied with permission [58]. Copyright 2013, the Nature publishing group.

firm fixation while allowing removal without significant damage to the tissue. In addition, dissimilar to unbending MNs, the powerful dynamic shape alteration properties of ES-HFMs keep them from bursting when eliminated from the tissue. Furthermore, Eun Young Jeon *et al.* designed mutually cross-linked biphasic ES-HFMs, involving a water-absorbable adhesive exterior based on swellable mussel adhesive protein and a rigid interior consisting of non-swellable silk fibroin-based core [32]. With excellent tissue insertion, surface adhesion and mechanical interlocking ability, the device achieves superior wound sealing capacity *in vitro* (139.7 ± 14.1 mmHg), comparable to clinically used sutures (151.0 ± 23.3 mmHg), offering immediate closure of bleeding intestinal wounds *in vivo* without leakage, abscesses or bowel obstruction.

Interestingly, Wei Chen *et al.* described an intelligent targeted capsule system that combines physical (MN) and non-physical (enhancer) drug delivery modes [106]. To build smart MNs with extension and tissue penetration, the dynamic omnidirectional adhesive MN system (DOAMS) featuring a biphasic core-shell structure, a soft outer layer (Carbopol) and a rigid inner core (polycaprolactone), was designed inspired by the natural thorny-headed intestinal worm (Fig. 10A). Afterward, a self-triggering capsule was designed inspired by the "jack-in-the-box" system, which delivers a

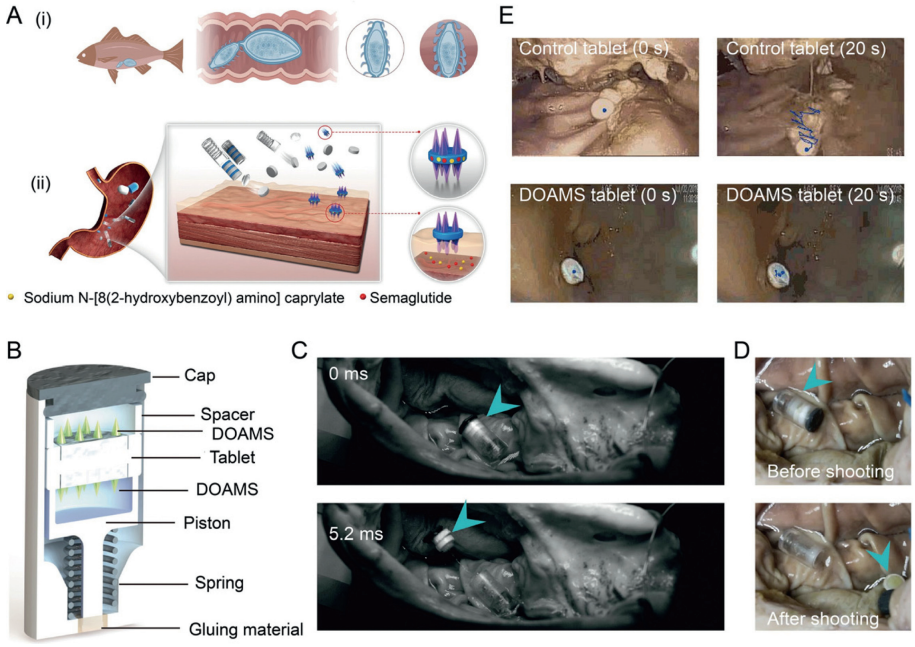

Fig. 10. Application of ES-HFMs for mechanical interlocking based on thorny-headed worm. (A) (i) Thorny-headed worm attaches to the intestine of fish. (ii) The microneedle-like structures in the head of the worm expand as they penetrate the intestine, providing strong adhesion. (iii) After intake, the "jack-in-the-box" system would automatically deploy into the tissues in reaction to the low pH environment in the stomach. (B) Schematic diagram of a device comprising a double DOAMS modified tablet. (C) The image display device from the high-speed camera is successfully triggered. (D) Pictures of the state of the double DOAMS modified tablets before and after initiation. (E) Endoscopic images showing the movement of control and individual DOAMS-modified tablets in the pig stomach. Copied with permission [106]. Copyright 2022, the Science Advances.

tablet loaded with MNs to the stomach, and then ejects it into the stomach cavity when triggered by the local gastric environment (Fig. 10B). DOAMS showed extremely high adhesion to *in vitro* pig stomach tissue (0.25 N), even stronger than commercial Carbopol powders (0.18 N). *In vivo,* real-time endoscopic imaging showed that conventional tablets (non-mucosal adhesives and non-MNs) migrated more than 30 mm in 20 s, while DOAMS-modified tablets stayed securely in place (Figs. 10C-E). This might be attributed to the presence of multiple interlocking mechanisms among DOAMS and the tissue: mechanical interlocking driven hooks and chemical adhesion of the hydrogel bonds between Carbopol and the tissue.

4. Challenges and perspective

The extraordinary dynamic shape variability and interaction tunability of ES-HFMs address a critical headway over customary MNs frameworks, enormously broadening the scope of MNs applications. Nevertheless, still lots of issues remain to be clarified for further clinical translation and commercial application of ES-HFMs. (1) The variability among individual patient groups, (*e.g.,* differences of water content in the skin of children, the elderly and pregnant women), poses a harsh challenge to precisely modulate the expansion coefficient and acting duration of ES-HFMs for personalized treatment. (2) Although the hydrogel polymers are produced with adequate cross-linking extent, undesired degradation may still occur during long-term action *in vivo*, thus worsening the inflammatory response in wet wounds. (3) MNs penetrating the stratum corneum are expected to avoid the introduction of harmful microorganisms into the skin, which frequently triggers an inflammatory response [107–111]. Different from the metals and silica MNs that use autoclaving process, ES-HFMs are typically sterilized using ultraviolet light irradiation, which presents tremendous challenges for light-sensitive or protein-based macromolecule encapsulation [112–116]. (4) In cases where ES-HFMs are not applied immediately after fabrication, the bioactive drug molecules on the surface may decrease activity during room temperature storage [117–119]. (5) Owing to being in small-scale research in experimental animal models, ES-HFMs needed to be tested in large animal models or humans in the near future [120–122].

As MNs continue to progress in commercialization, there is a greater necessity to address the issues related to their translation from the lab to the market. (1) Predictably, the ES-HFMs are expected to act as a portable and integrated device, indicating a great potential to be applied to scenarios outside of the laboratory, such as home and hospitals. As an illustration, combining ES-HFMs with other cutting-edge technologies (*e.g.,* microactuators, biosensors and microfluidic chips) to create intelligent microsystems to integrate sample collection/analysis and drug deployment [123–128]. (2) It is especially vital to enrich the dynamic shape alteration properties of ES-HFMs in fitting them better to implant sites containing irregular geometric shapes. Shimon Unterman *et al.* designed a nanocomposite hydrogel with independently tunable rheological and mechanical properties, consisting of dextran aldehyde and poly(amido amine) dendrimer mixed with phyllosilicate nanoparticles [129]. It has been proven that these nanocomposite hydrogels with different aspect ratios in combination with MNs could be optimally implanted in wet, fluid and inverted environments. (3) The optimal ES-HFM shapes are required to satisfy the needs of different individuals because the penetration of ES-HFMs varies with age, skin condition, and the applied force during the treatment. (4) The majority of currently available microneedle products are more expensive than conventional blood-based sample extraction and subcutaneous formulation injection; therefore, decreasing the cost of ES-HFMs and achieving mass production are crucial steps forward in the industry. Despite existing difficulties, ES-HFMs have been verified to exhibit considerable potential for deep point-of-care sampling and smart drug deployment by overcoming the shortcomings of conventional MNs. It is undoubtedly

that ES-HFMs will continuedly serve as a promising candidate for smart biomedical applications in the clinical and industry in the future.

Declaration of competing interest

The authors declare that they have no known competing financial interests or personal relationships that could have appeared to influence the work reported in this paper.

Acknowledgments

This study was supported by the Fundamental Research Funds for the Central Universities (No. 5003510106), the National Natural Science Foundation of China (Nos. U21A20417, 31930067), and 1·3·5 Project for Disciplines of Excellence, West China Hospital, Sichuan University (No. ZYGD18002).

References

[1] I. Menon, P. Bagwe, K.B. Gomes, et al., Micromachines (Basel) 12 (2021) 435.
[2] Y. Hao, W. Li, X. Zhou, et al., J. Biomed. Nanotechnol. 13 (2017) 1581–1597.
[3] T. Waghule, G. Singhvi, S.K. Dubey, et al., Biomed. Pharmacother. 109 (2019) 1249–1258.
[4] Á. Cárcamo-Martínez, B. Mallon, J. Domínguez-Robles, et al., Int. J. Pharm. 599 (2021) 120455.
[5] Y. Mizuno, K. Takasawa, T. Hanada, et al., Biomed. Microdevices 23 (2021) 38.
[6] J. Xu, D. Xu, X. Xuan, H. He, Molecules 26 (2021) 5912.
[7] R. Jamaledin, C. Di Natale, V. Onesto, et al., J. Clin. Med. 9 (2020) 542.
[8] R.S.J. Ingrole, H.S. Gill, J. Pharmacol. Exp. Ther. 370 (2019) 555–569.
[9] P. Dardano, S. De Martino, M. Battisti, et al., Polymers (Basel) 13 (2021) 520.
[10] V. Yadav, P.K. Sharma, U.S. Murty, et al., Int. J. Pharm. 605 (2021) 120815.
[11] N.D. Sheybani, H. Yang, Chin. Chem. Lett. 28 (2017) 1817–1821.
[12] Y. Chen, X. Zhang, F. Liu, et al., Chin. Chem. Lett. 32 (2021) 441–444.
[13] M. Avcil, A. Çelik, Micromachines (Basel) 12 (2021) 1321.
[14] D. Kulkarni, F. Damiri, S. Rojekar, et al., Pharmaceutics 14 (2022) 1097.
[15] J.H. Jung, S.G. Jin, J. Pharm. Investig. 51 (2021) 503–517.
[16] J. Yang, X. Liu, Y. Fu, Y. Song, Acta. Pharm. Sin. B 9 (2019) 469–483.
[17] R. Amarnani, P. Shende, Biomed. Microdevices 24 (2021) 4.
[18] F.K. Aldawood, A. Andar, S. Desai, Polymers (Basel) 13 (2021) 2815.
[19] R.F. Donnelly, T.R. Singh, M.J. Garland, et al., Adv. Funct. Mater. 22 (2012) 4879–4890.
[20] Z. Xu, G. Liu, J. Huang, J. Wu, ACS Appl. Mater. Interfaces 14 (2022) 7680–7689.
[21] H. Chang, M. Zheng, X. Yu, et al., Adv. Mater. 29 (2017) 1702243.
[22] C.F. Guimarães, R. Ahmed, A.P. Marques, et al., Adv. Mater. 33 (2021) e2006582.
[23] S. Li, Y. Cong, J. Fu, J. Mater. Chem. B 9 (2021) 4423–4443.
[24] A. Rajput, M. Kulkarni, P. Deshmukh, et al., Drug Dev. Ind. Pharm. 47 (2021) 1713–1732.
[25] K. Aich, T. Singh, S. Dang, Drug Deliv. Transl. Res. 12 (2022) 1556–1568.
[26] N. Xu, M. Zhang, W. Xu, et al., Analyst 147 (2022) 1478–1491.
[27] R. Narayanaswamy, V.P. Torchilin, Molecules 24 (2019) 603.
[28] Z. Sun, C. Song, C. Wang, et al., Mol. Pharm. 17 (2020) 373–391.
[29] L. Barnum, J. Quint, H. Derakhshandeh, et al., Adv. Healthc. Mater. 10 (2021) e2001922.
[30] X. Chen, H. Yu, L. Wang, et al., ACS Biomater. Sci. Eng. 7 (2021) 4870–4882.
[31] Z. Yin, D. Kuang, S. Wang, et al., Int. J. Biol. Macromol. 106 (2018) 48–56.
[32] E.Y. Jeon, J. Lee, B.J. Kim, et al., Biomaterials 222 (2019) 119439.
[33] Q. He, R. Kusumi, S. Kimura, et al., Carbohydr. Polym. 237 (2020) 116189.
[34] Y. Xu, H. Chen, Y. Fang, J. Wu, Adv. Health. Mater. 11 (2022) 2200494.
[35] D.F.S. Fonseca, P.C. Costa, I.F. Almeida, et al., Macromol. Biosci. 20 (2020) e2000195.
[36] M. Zheng, Z. Wang, H. Chang, et al., Adv. Healthc. Mater. 9 (2020) e1901683.
[37] F. Meng, A. Hasan, M. Mahdi Nejadi Babadaei, et al., J. Adv. Res. 26 (2020) 137–147.
[38] Y. Liu, D. Li, J. Ding, X. Chen, Chin. Chem. Lett. 31 (2020) 3001–3014.
[39] Y. Han, X. Li, Y. Zhang, et al., Cells 8 (2019) 886.
[40] J.G. Turner, L.R. White, P. Estrela, H.S. Leese, Macromol. Biosci. 21 (2021) e2000307.
[41] G. Yang, M. He, S. Zhang, et al., Drug Dev. Ind. Pharm. 44 (2018) 808–816.
[42] J.G. Hardy, E. Larrañeta, R.F. Donnelly, et al., Mol. Pharm. 13 (2016) 907–914.
[43] Q.K. Anjani, A.D. Permana, Á. Cárcamo-Martínez, et al., Eur. J. Pharm. Biopharm. 158 (2021) 294–312.
[44] K. Peng, L.K. Vora, J. Domínguez-Robles, et al., Mater. Sci. Eng. C: Mater. Biol. Appl. 127 (2021) 112226.
[45] T. Sheng, B. Luo, W. Zhang, et al., Adv. Drug Deliv. Rev. 179 (2021) 113919.
[46] X. He, J. Sun, J. Zhuang, et al., Dose Response 17 (2019) 1559325819878585.
[47] P. Makvandi, M. Kirkby, A.R.J. Hutton, et al., Nanomicro. Lett. 13 (2021) 93.
[48] K. Ahmed Saeed Al-Japairai, S. Mahmood, S. Hamed Almurisi, et al., Int. J. Pharm. 587 (2020) 119673.
[49] I. Xenikakis, M. Tzimtzimis, K. Tsongas, et al., Eur. J. Pharm. Sci. 137 (2019) 104976.
[50] K.J. Hsueh, M.C. Chen, L.T. Cheng, et al., Comp. Immunol. Microbiol. Infect. Dis. 50 (2017) 78–87.
[51] Z. Zhou, M. Xing, S. Zhang, et al., Int. J. Pharm. 618 (2022) 121669.
[52] G. Ma, C. Wu, J. Control. Release. 251 (2017) 11–23.
[53] M. Araújo, J. Silveira, A. Sousa, et al., Biomater. Sci. 9 (2021) 6510–6527.
[54] H. Witte, Biomimetics (Basel) 7 (2022) 96.
[55] A.R. Dixon, I. Vondra, Materials (Basel) 15 (2022) 4587.
[56] C. Plamadeala, S.R. Gosain, F. Hischen, et al., Biomed. Microdevices 22 (2019) 8.
[57] K. Girija Sravani, R.K. Desala, P. Chand, et al., IEEE Trans. Nanobioscience 22 (2023) 237–244.
[58] S.Y. Yang, E.D. O'Cearbhaill, G.C. Sisk, et al., Nat. Commun. 4 (2013) 1702.
[59] A. Hou, B. Cohen, A. Haimovic, N. Elbuluk, Dermatol. Surg. 43 (2017) 321–339.
[60] S.H. Bariya, M.C. Gohel, T.A. Mehta, O.P. Sharma, J. Pharm. Pharmacol. 64 (2012) 11–29.
[61] L. Fan, X. Zhang, X. Liu, et al., Adv. Healthc. Mater. 10 (2021) e2002249.
[62] M.A. Lopez-Ramirez, F. Soto, C. Wang, et al., Adv. Mater. 32 (2020) e1905740.
[63] P.P. Samant, M.M. Niedzwiecki, N. Raviele, et al., Sci. Transl. Med. 12 (2020) eaaw0285.
[64] X. Zhang, G. Chen, F. Bian, et al., Adv. Mater. 31 (2019) e1902825.
[65] P.P. Samant, M.R. Prausnitz, Proc. Natl. Acad. Sci. U. S. A. 115 (2018) 4583–4588.
[66] R.F. Donnelly, K. Mooney, M.T. McCrudden, et al., J. Pharm. Sci. 103 (2014) 1478–1486.
[67] R. He, Y. Niu, Z. Li, et al., Adv. Healthc. Mater. 9 (2020) e1901201.
[68] R.F. Donnelly, M.T. McCrudden, A. Zaid Alkilani, et al., PLoS One 9 (2014) e111547.
[69] S. Chen, H. Matsumoto, Y. Moro-Oka, et al., ACS Biomater. Sci. Eng. 5 (2019) 5781–5789.
[70] Y. Lei, Y. Wang, J. Shen, et al., Sci. Adv. 8 (2022) eabl6449.
[71] Y. Sun, Q. Zhou, Y. Du, et al., Small 18 (2022) e2201656.
[72] M.J. Ostro, P.R. Cullis, Am. J. Hosp. Pharm. 46 (1989) 1576–1587.
[73] H. Chen, Y. Cheng, J. Tian, et al., Sci. Adv. 6 (2020) eaba4311.
[74] J. Liu, M. Qu, C. Wang, et al., Small 18 (2022) e2106172.
[75] W. Lyu, Y. Ma, S. Chen, et al., Adv. Healthc. Mater. 10 (2021) e2100785.
[76] R. Huang, X. Zhang, W. Li, et al., Adv. Sci. 8 (2021) e2100201.
[77] Y.S. Kim, D.K. Sung, W.H. Kong, et al., Biomater. Sci. 6 (2018) 1020–1030.
[78] S. Orman, S. Yol, H. Uzun, et al., J. Invest. Surg. 33 (2020) 97–105.
[79] I. Woodhouse, S. Nejati, V. Selvamani, et al., ACS Appl. Bio. Mater. 4 (2021) 5405–5415.
[80] V. Deineka, O. Sulaieva, N. Pernakov, et al., Mater. Sci. Eng. C: Mater. Biol. Appl. 120 (2021) 111740.
[81] K. Howk, J. Fortier, R. Poston, Ann. Vasc. Surg. 31 (2016) 186–195.
[82] S. García-Salinas, M. Evangelopoulos, E. Gámez-Herrera, et al., Int. J. Pharm. 577 (2020) 119067.
[83] J. Kim, S.W. Kim, S. Park, et al., Adv. Healthc. Mater. 2 (2013) 1525–1531.
[84] O. Hakimi, P.A. Mouthuy, A. Carr, Int. J. Exp. Pathol. 94 (2013) 287–292.
[85] K.A. Zink, J.C. Mayberry, E.G. Peck, M.A. Schreiber, Am. Surg. 77 (2011) 438–442.
[86] N. R, K. M, P. J, et al., Colloids Surf. B: Biointerfaces 182 (2019) 110339.
[87] H.C. Tsai, G.R. Chang, H.C. Fan, et al., BMC Vet. Res. 15 (2019) 191.
[88] R. Li, K. Liu, X. Huang, et al., Adv. Sci. 9 (2022) e2105152.
[89] J. Chi, X. Zhang, C. Chen, et al., Bioact. Mater. 5 (2020) 253–259.
[90] S. Lim, T.Y. Park, E.Y. Jeon, et al., Biomaterials 278 (2021) 121171.
[91] S.J. Marshall, S.C. Bayne, R. Baier, et al., Dent. Mater. 26 (2010) e11–e16.
[92] J. Shin, E.H. Kang, S. Choi, et al., ACS Biomater. Sci. Eng. 7 (2021) 4230–4243.
[93] C. Samarawickrama, A. Samanta, A. Liszka, et al., Cornea 37 (2018) 609–616.
[94] F.M. Kamer, J.H. Joseph, Arch. Otolaryngol. Head. Neck. Surg. 115 (1989) 193–197.
[95] C. Ma, J. Sun, B. Li, et al., Nat. Commun. 12 (2021) 3613.
[96] Y. Lin, Z. Chen, Y. Liu, et al., Drug Des. Devel. Ther. 16 (2022) 2707–2728.
[97] Y. Teng, X. Zhang, L. Da, et al., BMC Musculoskelet. Disord. 22 (2021) 571.
[98] O.E. Beidas, J.A. Gusenoff, Aesthet. Surg. J. 39 (2019) S85–s93.
[99] M. Byrne, A. Aly, Aesthet. Surg. J. 39 (2019) S67–S72.
[100] B. Krishnamoorthy, N. Shepherd, W.R. Critchley, et al., Interact. Cardiovasc. Thorac. Surg. 22 (2016) 161–167.
[101] A. Cromi, A.S. Laganà, F. Ghezzi, et al., Eur. J. Obstet. Gynecol. Reprod. Biol. 271 (2022) 112–116.
[102] B.J. Cole, E.T. Sayegh, A.B. Yanke, et al., J. Am. Acad. Orthop. Surg. 24 (2016) 83–95.
[103] C. Salyer, A. Spuzzillo, D. Wakefield, et al., J. Surg. Res. 267 (2021) 705–711.
[104] R. Zan, H. Wang, J. Ni, et al., ACS Biomater. Sci. Eng. 7 (2021) 5269–5278.
[105] E.J. Hyland, D. Maze, T. Lawrence, et al., Int. Wound J. 13 (2016) 878–879.
[106] W. Chen, J. Wainer, S.W. Ryoo, et al., Sci. Adv. 8 (2022) eabk1792.
[107] R.K. Sivamani, D. Liepmann, H.I. Maibach, Expert. Opin. Drug Deliv. 4 (2007) 19–25.
[108] D. Li, D. Hu, H. Xu, et al., Biomaterials 264 (2021) 120410.
[109] T.T. Nguyen, Y. Oh, Y. Kim, et al., Hum. Vaccin. Immunother. 17 (2021) 316–327.
[110] N.S. Rejinold, J.H. Shin, H.Y. Seok, Y.C. Kim, Expert Opin. Drug Deliv. 13 (2016) 109–131.
[111] J. Richter-Johnson, P. Kumar, Y.E. Choonara, et al., Expert Rev. Pharm. Out. 18 (2018) 359–369.
[112] H. Lu, S. Zada, L. Yang, H. Dong, Front. Bioeng. Biotechnol. 10 (2022) 851134.

[113] A.K. Gera, R.K. Burra, J. Funct. Biomater. 13 (2022) 81.
[114] P.R. Yadav, M.N. Munni, L. Campbell, et al., Pharmaceutics 13 (2021) 1132.
[115] F. Zhang, W. Bao, R. Li, et al., Biomater. Sci. 7 (2019) 4503–4507.
[116] K. Ita, Pharmaceutics 7 (2015) 90–105.
[117] A. Sivaraman, A.K. Banga, Drug Deliv. Transl. Res. 7 (2017) 16–26.
[118] N.N. Aung, T. Ngawhirunpat, T. Rojanarata, et al., Int. J. Pharm. 586 (2020) 119508.
[119] J.Y. Li, Y.H. Feng, Y.T. He, et al., Acta Biomater. 153 (2022) 308–319.
[120] X. Chen, L. Wang, H. Yu, et al., J. Control. Release 288 (2018) 173–188.
[121] R.F. Donnelly, D.I. Morrow, M.T. McCrudden, et al., Photochem. Photobiol. 90 (2014) 641–647.
[122] N.G. Oh, S.Y. Hwang, Y.H. Na, ACS Omega 7 (2022) 25179–25185.
[123] C.G. Li, C.Y. Lee, K. Lee, H. Jung, Biomed. Microdevices 15 (2013) 17–25.
[124] Z. Faraji Rad, P.D. Prewett, G.J. Davies, Beilstein. J. Nanotechnol. 12 (2021) 1034–1046.
[125] P.C. Pandey, G. Pandey, R.J. Narayan, J. Biomed. Mater. Res. B: Appl. Biomater. 109 (2021) 33–49.
[126] P. Bollella, S. Sharma, A.E.G. Cass, R. Antiochia, Biosens. Bioelectron. 123 (2019) 152–159.
[127] M. Jeyhani, V. Gnyawali, N. Abbasi, et al., J. Colloid. Interface Sci. 553 (2019) 382–389.
[128] S.T. Sanjay, W. Zhou, M. Dou, et al., Adv. Drug Deliv. Rev. 128 (2018) 3–28.
[129] S. Unterman, L.F. Charles, S.E. Strecker, et al., ACS Nano 11 (2017) 2598–2610.